Efficiency, Speed, and Scaling of 2D Passive Dynamic Walking

Mariano Garcia *
Dept. of Integrative Biology
University of California at Berkeley
Berkeley, CA 94720

Anindya Chatterjee
Engineering Science & Mechanics
Penn State University
University Park, PA 16802

Andy Ruina
Theoretical & Applied Mechanics
Cornell University
Ithaca, NY 14853

Abstract

We address performance limits and dynamic behaviors of the two-dimensional passive-dynamic bipedal walking mechanisms of Tad McGeer. The results highlight the role of heelstrike in determining the mechanical efficiency of gait, and point to ways of improving efficiency. We analyze several kneed and straight-legged walker designs, with round feet and point-feet. We present some necessary conditions on the walker mass distribution to achieve perfectly efficient (zero-slope-capable) walking for both kneed and straight-legged models. Our numerical investigations indicate, consistent with a previous study of a simpler model, that such walkers have two distinct gaits at arbitrarily small ground-slopes, of which the longer-step gait is stable at small slopes. Energy dissipation can be dominated by a term proportional to (speed)^2 from tangential foot velocity at heelstrike and from kneestrike, or a term proportional to (speed)^4 from normal foot collisions at heelstrike, depending on the gait, ground-slope, and walker design. For all zero-slope capable straight-legged walkers, the long-step gaits have negligible tangential foot velocity at heelstrike and are hence especially fast at low power. Some apparently chaotic walking motions are numerically demonstrated for a kneed walker.

---

*previous address: Dept. of Theoretical & Applied Mechanics, Cornell University, Ithaca, NY 14853

1   Introduction

High energetic efficiency and high speed are obviously useful for both biological and robotic loco-
motion. Towards the end of better understanding these aspects of nature's designs and perhaps
inspiring designs for faster or more efficient robots, we have studied a special class of walking
mechanisms. In particular, this paper examines some basic features related to: a) efficiency, and
b) speed, of downhill passive bipedal walking mechanisms. These mechanisms were first designed,
simulated and built by McGeer (1990a), who credits the "ballistic" double- and triple-pendulum
leg models of Mochon and McMahon (1980) for inspiration. This work continues our extension of
McGeer's studies of these remarkable devices to more complex mechanisms than those studied in
(Garcia et al. (1998a)).

The choice of studying this particular class of designs is motivated as follows. While walking
certainly involves muscular activity, high degree-of-freedom simulations based on energy minimiza-
tion or other optimization criteria generally predict limited muscle use in repetitive motions such
as walking (see Yamaguchi and Zajac (1990), Beckett and Chang (1973) and Collins (1995)).
EMG (electromyographic) studies have also shown relatively little electrical activity from muscle
use in walking (see, e.g., Basmajian and Tuttle (1973)). Thus controlled motor input might be
sensibly neglected in some analyses just as engine power is neglected for some studies of flight
(McGeer (1990a)). The use of gravity instead of motors simplifies experimental verification and
reduces the arbitrariness of the model. Our hope is that some of the results for gravity-powered
mechanisms, even if not a direct simulation of motor powered walking, will provide insight for more
complex powered and controlled systems. The extent to which humans, say, do and do not follow
the patterns described here is information about human design and control. Finally, whatever the
relevance to biology, these mechanisms are inherently intriguing.

1.1   Passive dynamic walking mechanisms

The general type of 2D walking mechanisms we study, essentially McGeer's design, is shown
schematically in figure 1. It consists of a *swing leg* (not in contact with the ground) and a *stance
leg* (rolling without slip on the ground), connected by a frictionless hinge at the *hip*. Extra mass is
added at the hip, in part serving as a crude model of an upper body. The two legs are identical;
each is composed of a rigid *thigh* and *shank*. The *stance knee* is locked. The *swing knee* is a fric-
tionless hinge with a knee-stop preventing hyperextension at *kneestrike*. When the swing leg foot
hits the ground at *heelstrike*, the legs interchange roles. The *straight-legged* version of this walker
is the same mechanism with permanently-locked knees. The details of the mass distribution and
its effects are discussed throughout the paper.

A strobe photo of one of our physical models is shown in figure 2. A simulated walking cycle,
using parameters measured from this model, is shown schematically in figure 3 and also compared
with kinematic data from human walking. No attempt was made to do any parameter matching
with the human data. In particular the human gait shown has larger leg swing angles.

McGeer-like passive mechanisms seem useful for both the study of human gait and robotics for
three reasons:

1. **Existence.** These vaguely anthropomorphic, uncontrolled legged mechanisms have human-
   like motions, suggesting that human walking may be based on, at some level of approximation,
   the uncontrolled motions of bars connected by hinges.

2. **Efficiency.** Machines of this type can walk down very shallow ground-slopes and thus have
   high energetic efficiency.

3. **Stability.** For certain parameter combinations, the passive mechanisms' gaits are stable. Such passive stability is available to be exploited by the control systems of robots and might well already be exploited by animal brains and reflexes.

Stable motions of different walkers were found by McGeer, and later by Goswami et al. (1996) and Garcia et al. (1996). However, unstable walking motions of passive walkers can in principle be stabilized with minimal (theoretically zero) energetic cost and simple control strategies. This has been demonstrated by McGeer (1993), Fowble and Kuo (1996), and Kuo and Bauby (1999). Because mildly unstable passive motions are easily stabilizable, and because animals and robots inevitably have some sensing, computing, and motor functions available, mildly unstable passive motions are possibly as relevant as passively stable ones. Thus we do not eliminate unstable motions from consideration here; however, biologically relevant or not, a numerical simulation model must be stable before the corresponding passive physical model can be expected to work as a demonstration.

1.2 The organization of the rest of this paper

We first discuss some of the tools used in the analysis, especially maps; next, we motivate our use of ground-slope γ as a measure of inefficiency. The results for a simpler walking model that this paper generalizes are then reviewed. Section 4 describes the general features of our numerical simulations. The remainder of the paper is a discussion of issues inspired by these simulations. The possibility of passive walking at arbitrarily small ground-slopes ("*zero-slope* walking") is discussed in section 5 and related to numerical verifications. In section 6, some basic scaling rules for zero-slope capable walkers are obtained analytically and compared with the numerical results. This work mostly subsumes that reported by Garcia et al. (1996), Garcia et al. (1997), and Garcia et al. (1998b).

2 Preliminaries

2.1 The step-to-step map and limit cycles

Gait analysis lends itself to study with Poincaré maps because of the clear ground collision (heel-strike) events. This approach seems to have been first used by Hurmuzlu and Moskowitz (1986) for walking in general and by McGeer for passive machines like those we study here. Garcia (1999), Coleman et al. (1997) and Coleman (1998) review the techniques used and we briefly summarize them below for completeness.

The motions of the walker are governed by standard rigid body dynamics. In our way of formulating these, all of the equations described below are based on angular momentum balance about various points. A walking step starts right after heelstrike, just when the old stance leg (which is now the swing leg) starts swinging. Equations of motion for the *three-link mode* are integrated forward in time until kneestrike is detected. Assuming no rebound (perfectly plastic knee collision), jump conditions then determine the post-kneestrike state. Equations of motion for the *two-link mode* are now integrated forward in time until heelstrike is detected. Assuming no rebound (perfectly plastic heel collision) and no ground impulse at the trailing foot, jump conditions are used to determine the post-heelstrike state from the pre-heelstrike state. This completes one walking step. Details of derivations of the various equations needed to simulate each step are available in McGeer (1990a) as well as Garcia (1999) and Coleman (1998).

For readers familiar with clinical terminology, our model has an instantaneous *double-support phase.* In our mathematical model, the kneestrike and heelstrike collisions are instantaneous, while in our aluminum physical model, they are very brief (perhaps tens of milliseconds). In human

walking, kneestrike and heelstrike durations are somewhat longer, but still significantly shorter than the gait period.

Each step is viewed as one evaluation of a map. The state $^i\boldsymbol{\theta} = {}^i\{\theta_{st} \ \theta_{th} \ \theta_{sh} \ \dot\theta_{st} \ \dot\theta_{th} \ \dot\theta_{sh}\}$ is mapped, one step later, to $^{i+1}\boldsymbol{\theta}$. We abstractly define this map

$$^{i+1}\boldsymbol{\theta} = \mathbf{f}(^i\boldsymbol{\theta}). \tag{1}$$

(McGeer termed this step-to-step map the "stride function.") Evaluating the map $\mathbf{f}$ generally requires *numerical* solution of differential equations to a termination condition and then *numerical* evaluation of the jump condition (matrix multiplication). Although it is a task to assemble the computation, the net result is represented by the simple equation 1.

Straight-legged walkers are always in two-link mode, have no kneestrike, and $\boldsymbol{\theta}$ simplifies to $\{\theta_{st} \ \theta_{th} \ \dot\theta_{st} \ \dot\theta_{th}\}$.

If the new initial conditions after one step are exactly the same as those of the previous step, we have a fixed point of the map $\mathbf{f}$, or a *gait cycle* (which is a period-one limit-cycle). We denote gait cycle initial conditions with an asterisk. Thus $\mathbf{f}(\boldsymbol{\theta}^*) = \boldsymbol{\theta}^*$, and θ_{st}^* is the stance angle at the start of a gait cycle.

If a gait cycle exists, it might be stable, in which case it can be found by direct simulation of the system over several steps, provided the initial conditions lie in the basin of attraction (as in Goswami et al. (1997)). Whether stable or not, fixed points can be found as in McGeer (1990a) using root-finding algorithms to find the zeros of $\mathbf{g}(\boldsymbol{\theta}) \equiv \mathbf{f}(\boldsymbol{\theta}) - \boldsymbol{\theta}$. At the fixed point, the eigenvalues of the Jacobian of $\mathbf{f}$ determine stability (having all eigenvalue magnitudes less than unity guarantees local asymptotic stability).

Given an n dimensional map definition $\mathbf{f}$, like above, finding a periodic solution $\boldsymbol{\theta}^*$ comes down to solving n equations in n unknowns, namely $\mathbf{f}(\boldsymbol{\theta}^*) = \boldsymbol{\theta}^*$. But there is no *a priori* guarantee, for an arbitrary set of walking mechanism parameters (i.e., masses, lengths, and ground-slope), that such a $\boldsymbol{\theta}^*$ exists, or that there might not be more than one solution, or that any solutions correspond to reasonably anthropomorphic motions. Non-anthropomorphic walking solutions, where, for example, the swing leg swings forward and backward more than once per step, can exist (see Garcia et al. (1998a) and Coleman (1998)), but we eliminate them from our simulations.

2.2 The dimension of the map f

In general, one expects the dimension of a Poincaré map to be one less than the dimension of the phase space of the system. For general straight-legged walkers, the map of the 4th-order system (two angles and two rates) is generally three-dimensional. For the superficially 6th-order kneed walker (three angles and three rates in three-link mode), the map is also only three-dimensional because the kneed walker is like a straight-legged walker during two-link mode, and its state during this (4th-order) mode determines all future states in both two and three-link modes. Thus, for example, of the four numerically-evaluated eigenvalues of McGeer (1990b) (reported as $-0.001, 0.073, 0.261 \pm 0.363i$), the first is (exactly) mathematically zero.

2.3 Measures of efficiency

Finding a rational dimensionless measure of energetic efficiency for transport or locomotion on level ground is somewhat problematic. Because moving sideways in a gravitational field is ideally workless, the most reasonable measure of efficiency

$$\frac{\text{(fundamental minimum energetic cost)}}{\text{(actual cost)}} \tag{2}$$

is zero except when it is undefined (0/0). The common dimensionless measure of (in)efficiency for locomotion is the "specific cost of transport"

$$\eta = \frac{\text{(mechanical energy cost for transport)}}{\text{(weight)} \times \text{(distance traveled)}} \tag{3}$$

where the energy cost is also the energy dissipated. Taking the distance as one step, this reduces to (McGeer (1993))

$$\eta = \frac{\text{(energy dissipated per step)}}{\text{(walker weight)} \times \text{(step length)}} \ . \tag{4}$$

For gravity-powered walking, the energy dissipated is (weight) × (height drop over one step). So, based on horizontal distance, or path distance, the inefficiency measure is, respectively

$$\eta = \tan\gamma \qquad \text{or} \qquad \eta = \sin\gamma \tag{5}$$

where γ is the ground-slope.

Rolling resistance, friction coefficient, and airplane glide ratio are other similar ratios which relate vertical support force to forward (propulsive) force necessary to maintain constant forward velocity. For downhill locomotion on small ground-slopes, we can thus equate many reasonable inefficiency measures to

$$\text{inefficiency} = \gamma. \tag{6}$$

Perfect transport efficiency is achieved by passive walking with $\gamma = 0$.

Note that energetic efficiency does not credit speed, which is also important for animals and machines. Intuitive measures of merit, such as minimizing power for a given speed, are dimensional, and thus lead to improvement by scale changes alone. A simple nondimensional measure of merit that rewards speed is the square root of the Froude number, or nondimensional velocity

$$\frac{v}{\sqrt{gl}} \tag{7}$$

at a fixed ground-slope which cannot be affected by simple scaling changes. The scaling results here are reported using angle θ_{st}. In our scaling arguments for a given gait, the period is roughly independent of γ and θ_{st} is small, so both step length and nondimensional velocity scale with θ_{st}. However, θ_{st} is not a proxy for nondimensional velocity when comparing distinct gaits with differing periods.

3   Review of the Simplest Walker

An extreme simplification of a straight-legged walker is the "minimal biped" of Alexander (1995), a hip-mass with controlled massless legs with point-feet. This model is made passive and mechanically deterministic by the addition of infinitesimal point-masses at the feet so that the legs swing with no control. This parameter-free mechanism was studied in some detail both numerically and analytically by Garcia et al. (1998a). We summarize those results here because the present paper generalizes them.

The simplest walker has two period-one gaits for all positive ground-slopes (up to 0.2 rad$\approx 12°$ and possibly higher). The long-step gait also has a longer period and is somewhat relaxed in

nature, with the swing leg swinging forward and back a little before heelstrike. The short-step gait has a shorter period and a truncated shuffling aspect, since heelstrike occurs as the swing leg is still swinging forward. Of these two, the *long-step* gait is stable at sufficiently small ground-slopes ($\gamma < 0.015$), while the *short-step* gait is always unstable (in Garcia et al. (1998a) these two gaits are called the "long-period" and "short-period" gaits, but in this paper we use "long-step" and "short-step" instead).

As $\gamma \to 0$, the long-step gait approaches a time-reversal-symmetric motion with normal heel-strike collisions ($\dot{x}/\dot{y} \to 0$ as $\gamma \to 0$ in figure 4, where $\dot{y}$ and $\dot{x}$ are the x and y velocities of the foot contact point at the instant prior to heelstrike). The short-step gait lacks this time-reversal symmetry, and the pre-heelstrike foot velocity has a significant tangential ($\dot{x}$) component.

For this walker, both gait cycles were found to have walking speed and stance angle θ_{st} (nondi-mensionalized step-length) each proportional to $\gamma^{1/3}$ as $\gamma \to 0$, while the step periods approach nonzero constants. Thus, at low speeds of the simplest walker, walking power consumption is proportional to the fourth power of speed for *both* gaits:

$$\text{Power} \propto mv^4 g^{-1/2} l^{-3/2}, \tag{8}$$

where m is the walker mass, v is the average walking velocity, g is the gravitational constant, and l is the walker's leg length. This scaling also follows from the energy balance between collision loss per step and used-up gravitational potential energy, along with the observation that step period is roughly independent of ground-slope (discussed in detail in section 6 here and also by Garcia et al. (1998a)). A key feature of *this* model is that the collision losses are all from deflection of the hip mass. Because the foot mass is infinitesimal, the tangential aspect of the collision makes no contribution to dissipation. The proportionality constants in equation 8 are different for the two gaits because they have different step lengths and periods. For the simplest walker, the short-step gait is faster (has bigger average velocity v) than the long-step gait at all ground-slopes studied.

For $0.015 \lesssim \gamma \lesssim 0.019$ a period-doubling route to chaos was observed for this walker. Howell and Baillieul (1998) have discovered an unconnected stable period-three branch of gaits at $\gamma \approx 0.0125$ and subsequent period-doublings (period-six, period-twelve, etc.). Note that there is thus a range of γ values where a stable period-one gait cycle coexists with an unstable period one gait cycle and a stable period-three gait cycle. Further, there are two disconnected chaotic regimes. Besides their curiosity value, such complex passive walking motions suggest the existence of passive-dynamics-dominated variable gaits (e.g., limping, waltzing, and staggering) in humans and robots.

4   Simulation of More Complex Walking Models

We now present numerical results for more general walkers. The equations of motion used here were derived using symbolic algebra (Maple), and solved numerically using Matlab. The numerical methods and error checks used were similar to those described in Garcia et al. (1998a).

4.1   Straight-legged point-foot walker with non-negligible foot mass

The dimensionless mass distribution of each leg of a straight-legged walker is given by its center of mass position and radius of gyration. In the studies of point-foot walkers by Goswami et al. (1996) and Goswami et al. (1997), the center of mass was on the foot-to-hip line (zero fore-aft offset), reducing the number of dimensionless parameters from 3 to 2. Here, we first consider a subset of those walkers, with simply a large mass at the hip and a small (but finite) mass at the foot, further reducing the number of parameters by one. As with the simplest walker, the location of

the second point-mass exactly on the foot ensures that the return map is two-dimensional because the swing leg makes no contribution to the just-before-heelstrike system angular momentum about the impending heelstrike point (see Garcia et al. (1998a)).

Solution families and scaling laws

Like the simplest walker, these walkers have two gait solutions at small ground-slopes. The two solutions are distinguished by the long-step solution having essentially normal heelstrike collisions $\dot{x}/\dot{y} \ll 1$ in figure 4) and the short-step solution having heelstrike collisions with a significant tangential component ($\dot{x}/\dot{y} \gg 1$ in figure 4). This pattern was also approximately observed in McGeer (1992) for more complex walkers, as well as for the "silly wheel" of McGeer (1993), which is a straight-legged walker whose semicircular foot is centered at the hip. For McGeer's silly wheel, the long period gait corresponds to support transfer when angles and rates are matched, much like a rolling wheel.

For the simplest walker, with *infinitesimal* foot mass, the only kinetic energy lost is that of the hip. When the feet have finite mass, however, the swing foot also loses energy when it hits the ground at heelstrike. For the long-step gait, where the swing foot collides with essentially no tangential velocity, the energy loss scales as step length to the fourth power, and step length is proportional to $\gamma^{1/3}$ as for the simplest walker. However, the short-step gait, with non-negligible tangential collisions at heelstrike, is slower at very small ground-slopes, having step length proportional to γ. Figure 5 shows stance angle as a function of γ for both solutions for two such walkers. In the figure, the long-step solution's stance angle is proportional to the cube-root of the ground-slope (like the simplest walker). Unlike the simplest walker, the short-step solutions' stance angles are proportional to γ at very small ground-slopes, and approximately to $\gamma^{1/3}$ at ground-slopes above some threshold γ that depends on foot mass. At these higher ground-slopes, the short-step solution is the faster solution (as was the case for all ground-slopes with the simplest walker).

The short-step transition region

The ground-slope at the transition from linear to cube root scaling of the short-step gait is governed by the ratio of the foot mass to the total mass. If the foot mass is ρ times the total mass, then the transition is numerically observed to occur at about a ground-slope proportional to $\rho^{3/2}$; step length is proportional to $\gamma^{1/3}$ for $\gamma \gg \rho^{3/2}$, and step length is proportional to γ for $\gamma \ll \rho^{3/2}$.

See the loglog plot in figure 5 where two such transitions are shown. Above the transition region, foot mass effects are unimportant, and the short-step gaits of both walkers follow similar $\gamma^{1/3}$ curves. Walker E has a foot-to-total mass ratio $\rho_E = 0.1$. Walker F has a foot-to-total mass ratio $\rho_F = 0.05$. The transition scaling predicts that the transition γ for walker E should be centered around $C \times \rho_E{}^{3/2} = 0.1^{3/2}\, C \approx 0.032\, C$ for some constant C; and that of walker F centered around $C \times \rho_F{}^{3/2} = 0.05^{3/2}\, C \approx 0.011\, C$. Instead of evaluating C and checking its constancy we find the intersections of linear extrapolations of the small-ground-slope portions of the gait curves with the (nearly identical) $\gamma^{1/3}$ lines corresponding to the larger-ground-slope scaling for each walker. The ratio of the two intersection γ values is predicted, for constant C, to be $(\rho_E/\rho_F)^{3/2}$ as approximately observed in figure 5.

In section 6, we will provide an analytical derivation of this $3/2$ power scaling for the transition.

4.2   A less special kneed and straight-legged walker

Figures 2 and 3, and the caption therein, show our near-duplicate of McGeer's walker in configuration, construction, and mass distribution (McGeer (1990b)). Figure 6 shows calculated stance angle

θ_{st} at gait cycles occurring at different ground-slopes γ. Three lab measurements of our physical walker are also shown. The dashed curve shows simulated stance angle versus ground-slope for the straight-legged walker, defined as this kneed walker with the knees locked. For some (simulated) solution regions on this plot, we allow various non-physical phenomena, like the swing foot passing through the ground, which are detailed and excused in appendix A.

Some observations about the solutions in figure 6 and our other simulations

1. For the set of simulations in fig. 6, the straight-legged gaits (dashed lines) are unstable and only a part of the kneed gait (solid line) is stable. In general, we find at most one stable period-one solution for a given set of design parameters and ground-slope.

2. Going up the kneed curve from point 3, kneestrike occurs later and later in the step, until heelstrike and kneestrike occur simultaneously at point 1. The locus of gaits ends here because we do not allow heelstrike to precede kneestrike. In the analogous region for the straight-legged walker (dashed), approaching point 2, the heelstrike collision becomes increasingly tangential in nature, until the solution disappears due to the swing foot never re-emerging from under the ground surface. In general, solution curves end at points where one or another condition for walking marginally fails.

3. Approaching points 3 and 4 the gait cycles slow down and eventually end. The straight-legged solutions approach zero step length. The kneed solutions approach a gait where kneestrike occurs immediately after heelstrike (initial swing shank and swing thigh velocities are such that the swing leg would hyperextend immediately after heelstrike, a motion we disallow). Points 3 and 4 are the slowest gaits for both walkers. For these walkers, the slowest walking is not at the smallest ground-slope.

4. The walkers of figure 6 have no solutions below some minimum ground-slope, ($\gamma_{\min} \approx 0.016$ for the straight-legged walker and $\gamma_{\min} \approx 0.020$ for the kneed walker).

5   Walking at Near-Zero Slopes

Generic McGeer-like walking mechanisms, like the ones just discussed, typically have no steady walking motions below some nonzero ground-slope; thus, they have some inherent nonzero inefficiency. But the point-foot walker with negligible or non-negligible foot mass can walk on arbitrarily small ground-slopes. We now consider the possibility of more general straight-legged and kneed walkers being capable of walking at arbitrarily small ground-slopes.

5.1   Necessary conditions on mass distribution for zero-slope walking

As demonstrated in a companion paper by Chatterjee and Garcia (1999), any McGeer-like walking mechanism that is capable of walking on very small ground-slopes must do so slowly (as $\gamma \to 0$ so must $v \to 0$). For the slow motions at near-zero-slope walking, gravity forces dominate over inertia forces. As a result, the walker must be close to static equilibrium at all times. In the limit of infinitesimal steps on an infinitesimal ground-slope, the walker configuration must approach static equilibrium standing on one leg. Further, in this configuration the knee must be on the boundary between locked and unlocked. Finally, pivoting of the swing leg must not cause interpenetration (to first order) or heelstrike could not be obtained. This gives us the following necessary conditions on the geometry and mass distribution of a 2D walker with equal legs for which zero-slope walking

might be possible. The mechanism must have a configuration where, with parallel legs and both feet touching the ground without interpenetration (see figures 7(a) and (b)):

1. The foot contact, the hip hinge and the total center of mass (cm) are collinear on a line that is orthogonal to the ground (for circular feet, the foot center is also on the ground-hip-cm line);

2. For kneed walkers the line connecting the knee hinge and the shank center of mass is parallel to the ground-hip-cm line and the knee stop must be at the boundary of engagement.

These statics-based necessary conditions on the mass distribution do not guarantee that zero-slope walking solutions exist and we do not know sufficient conditions that guarantee such solutions. In our simulations, however, designs which meet the necessary conditions, and whose center of mass is close to the hip, have walking motions for arbitrarily small ground-slopes.

The mechanisms investigated by Goswami et al. (1996) and Goswami et al. (1997) satisfy these necessary conditions, and presumably walk at arbitrarily small ground-slopes.

5.2   Tuning mass-distribution for zero-slope walking

The walkers of figure 3, whose loci of solutions are shown in figure 6, can be mathematically "deformed" (by parameter changes) into walkers that meet the statics conditions for zero-slope walking described above. We found numerically that both of these *tuned* walkers do indeed have walking motions at near-zero-slopes. In these numerical experiments, some inequality conditions are violated (see appendix A), and so one cannot experimentally verify the very small ground-slope walking for these models without adding some minimal actuation or control. These solution sets have similar natures to the solution sets for the simplest walker: each walker has two gait cycles at all ground-slopes of $\gamma < 0.04$; the long-step, long-period cycle is stable at small ground-slopes, while the short-step, short-period cycle is unstable. Thus the curves of figure 6 may be viewed as somewhat deformed versions of those reported for the simplest walker in Garcia et al. (1998a). In particular, the plots in figure 8 show the evolution of the solution curves of the tuned kneed walker (figure 7) as it is detuned into the original kneed walker of figure 6. As the zero-slope-capable walker is detuned, the graphs change shape in the following ways.

1. In figures 6(b)-(d) the cusp at the origin breaks and the two solutions separate. The long-step solution remains stable for small ground-slopes but shifts to the right and no longer extends to zero ground-slope. Also, an unstable region appears on this branch at very low speeds.

2. The short-step solution also shifts to the right; the point on this curve where the solution terminates (where heelstrike and kneestrike are simultaneous) shifts up the more or less same-shaped curve.

3. At higher ground-slopes, figures 6(d)-(e), the two solution branches get closer and eventually touch at some critical detuning value; the curves then split into two new solution branches. As the walker is de-tuned further, the solutions continue to separate. The high-ground-slope solution branch presumably continues to exist at still higher ground-slopes than shown in figure 6(f).

5.3   Zero-slope walkers

Figure 11 shows short-step and long-step gait solutions for the above mentioned tuned straight-legged (A) and kneed (C) walkers, the point-foot walker of Garcia et al. (1998a) (D), which is tuned

by definition, and two other tuned straight-legged models (B and E). The parameters for each of these tuned walkers are listed in the table of figure 9. Both linear and log-log plots of the data are shown.

We observe the following:

1. All of these walkers can walk at arbitrarily small ground-slopes.

2. The simplest walking model (D) is the only one with both gaits having a step length $\propto \gamma^{1/3}$. That is, the short step solution shown in figure 8(a) actually has a qualitative difference from the corresponding plot for the simplest walker in Garcia et al. (1998a) in that the short step solution is linear rather than cube-root near the origin.

3. At the smallest ground-slopes, the tuned straight-legged walkers with finite foot mass (A, B, and E) each have one gait solution with step length $\propto \gamma$ (the short-step gait) and one solution with step length $\propto \gamma^{1/3}$ (the long-step gait). At steeper ground-slopes ($\gamma > 0.01$), all the gait solutions have step length $\propto \gamma^{1/3}$ as seen most clearly in figure 11(b). In section 6, we explain these scaling patterns further.

4. The tuned kneed walking solutions (C) *seem* to follow a similar pattern to the straight-legged solutions in figure 11 at small ground-slopes. However, the long-step lengths of the tuned kneed walker are not proportional to $\gamma^{1/3}$ at *very* small ground-slopes. (Note how the kneed gait curve trails off at the left of the plot.) Numerical results indicate that this solution slowly changes to a linear scaling at extremely small ground-slopes ($\gamma \approx 0.00015$). Strictly speaking then, for the kneed walker, both the long-step and short-step gaits have step lengths $\propto \gamma$, although the longer period gait changes its scaling from cube root to linear at extremely small ground-slopes.

5. Although it is not shown in the plots, all of the tuned long-step gaits have a certain ground-slope below which the gait is stable (down to zero ground-slope).

Given that period is a weak function of γ, energy balance shows that for gaits with step length $\propto \gamma^{1/3}$, gravitational power consumed is $\propto (\text{speed})^4$, while for gaits with step length $\propto \gamma$, power $\propto (\text{speed})^2$. Thus, for a given small speed, the long-step gaits are much more efficient than the short-step gaits.

6   Energy Calculations and Scaling for Near-Zero-Slope Walking

In this section, we derive the scaling rules which we demonstrated above with numerical simulations. The key to this discussion is calculation of collisional dissipation, particularly at heelstrike. Because kneed walkers have their knees locked at heelstrike, the discussion starts only with straight-legged walkers.

6.1   The contact mass matrix

We review here the contact mass matrix for collisions (see, e. g., Brach (1991), Brogliato (1996), Chatterjee (1997) and Chatterjee and Ruina (1998) for more details and references).

Neglecting Coriolis, centripetal, and gravitational terms, the acceleration $\mathbf{a}_C$ of the impending contact point C in figure 4 is related to a possible finite contact force $\mathbf{F}$ by

$$\mathbf{F} = \mathbf{M}\mathbf{a}_C \ ,$$

where $\mathbf{M}$ is the (generally not isotropic) contact mass matrix. Calculation of the work absorbed by this force in a collision of vanishingly short duration implies that, if the velocity of C just before collision is $\dot{x}$ down the slope and $\dot{y}$ normal to the ground-slope as in figure 4, then the energy lost in an inelastic ($\dot{x}_{\text{after}} = \dot{y}_{\text{after}} = 0$) collision is

$$\text{heelstrike energy loss} = \frac{1}{2} \begin{bmatrix} \dot{x} & \dot{y} \end{bmatrix} \underbrace{\begin{bmatrix} M_{11} & M_{12} \\ M_{21} & M_{22} \end{bmatrix}}_{\mathbf{M}} \begin{bmatrix} \dot{x} \\ \dot{y} \end{bmatrix} \ . \tag{9}$$

In general $\mathbf{M}$ is a 2×2, symmetric, positive semi-definite (generically definite) matrix and thus has two mutually orthogonal eigenvectors. $\mathbf{M}$ depends on the parameters of the walker as well as its configuration (i.e., on θ_{st}). At heelstrike, $\theta_{st} = \theta_{th}$. The collision contact inertia matrix $\mathbf{M}$ is a function of θ_{st}, but since θ_{st} is small we write

$$\mathbf{M}(\theta_{st}) = \mathbf{M}(0) + \mathcal{O}(\theta_{st}). \tag{10}$$

where $\mathbf{M}(0)$ is $\mathbf{M}$ in the limit as $\theta_{st} \to 0$.

For zero-slope-capable walkers, a vertical force $\mathbf{F}$ on the walker will cause the entire walker to accelerate in the y (or 1) direction. Thus the y direction is an eigenvector of $\mathbf{M}$, the (x, y) coordinate system diagonalizes $\mathbf{M}$, and $M_{11} = m_{\text{tot}}$, the total mass of the walker. The x (or 2) direction is also an eigenvector and M_{22} is smaller than M_{11}. For a straight-legged, point-foot walker with a small foot mass (as considered in subsection 4.1), M_{22} is (asymptotically for small foot mass and as the stance angle goes to zero) equal to the foot mass. Note that, since the x and y directions are eigenvector directions, we have $M_{12} = M_{21} = 0$, i.e., $\mathbf{M}$ is diagonal. It follows that the energy dissipated in the foot collision is asymptotically equal to

$$\text{heelstrike energy loss} = \frac{1}{2} M_{11} \dot{x}^2 + \frac{1}{2} M_{22} \dot{y}^2 \ . \tag{11}$$

6.2 Derivation of scaling rule for straight-legged walkers

Now we express $\dot{x}$ and $\dot{y}$ in terms of $\dot{\theta}_{st}$ and $\dot{\theta}_{th}$, at the heelstrike configuration but just before heelstrike during a gait cycle ($\theta_{th} = -\theta_{st}$, and/or x and y small in figure 4). Defining the length l to be the distance between the hip and the foot center, we obtain:

$$\begin{aligned} \dot{x} &= R(\dot{\theta}_{st} - \dot{\theta}_{th}) + l \cos\theta_{st}(\dot{\theta}_{st} - \dot{\theta}_{th}), \\ \dot{y} &= -l \sin\theta_{st}(\dot{\theta}_{st} + \dot{\theta}_{th}). \end{aligned} \tag{12}$$

Assume that as $\gamma \to 0$, the gait cycle's nondimensional step length θ_{st}^* is asymptotically of $\mathcal{O}(\gamma^p)$ for some $p > 0$. During the walking step, the angular rates $\dot{\theta}_{st}$ and $\dot{\theta}_{th}$ must also be $\mathcal{O}(\gamma^p)$; at heelstrike, one or both of these angular rates are also of the same order of magnitude $\mathcal{O}(\gamma^p)$. One therefore expects, from equation 12, that the foot velocity components scale as

$$\dot{x} = \mathcal{O}(\gamma^p) \ \text{ and } \ \dot{y} = \mathcal{O}(\gamma^{2p}). \tag{13}$$

Typically, the energy loss in the collision (from equation 11) is therefore $\mathcal{O}(\gamma^{2p})$. Since the potential energy available per step is $\mathcal{O}(\gamma^{p+1})$ (step length × ground-slope), the energy balance requires that $2p = p + 1$, or $p = 1$, i.e., the step length is proportional to γ.

On the other hand, for some gaits of some walkers it may happen that, to leading order (i.e., to $\mathcal{O}(\gamma^p)$), $\dot{x} = 0$, or $\dot{\theta}_{st} - \dot{\theta}_{th} = 0$. In such cases, the energy dissipation per step is $\mathcal{O}(\gamma^{4p})$. As before, the potential energy available per step is $\mathcal{O}(\gamma^{p+1})$. Energy balance therefore requires $4p = p + 1$, or $p = 1/3$, i.e., the step length *can* be proportional to $\gamma^{1/3}$. Thus, it is seen that the only two possibilities for step lengths proportional to γ^p are $p = 1$ and $p = 1/3$.

The key to the argument above is the observation, made previously by Alexander (1995) for the minimal biped and McGeer (1990a) for the rimless wheel, that, from equation 12 the normal velocity at heelstrike scales with $\theta_{st} \times \dot{\theta}_{st}$ and not just $\dot{\theta}_{st}$.

6.3   The short-step power law transition ground-slope for point-foot walkers

Short-step gaits for straight-legged walkers with small but non-negligible foot masses and point-feet will typically exhibit a transition region between the linear and cube-root scalings, as discussed in section 4.1. Consider the effect of a small foot mass of ρ times the total mass (here assumed nondimensionalized to unity), on the simplest point-foot walker. That is, $M_{11} = 1$ and $M_{22} = \rho + \text{h.o.t.}$

For small θ_{st} as above, the kinetic energy dissipated in the collision is, to leading order in ρ,

$$\frac{1}{2}\left(\dot{y}^2 + \rho \dot{x}^2\right).$$

Assuming a step length comparable to γ^p as before, we find that energy balance requires

$$\gamma^{p+1} = \mathcal{O}(\gamma^{4p} + \rho \gamma^{2p})$$

or

$$\gamma^{3p-1} + \rho \gamma^{p-1} = \mathcal{O}(1).$$

For ρ small but fixed, this expression implies $p = 1$ as γ becomes arbitrarily small (i.e., step length $\propto \gamma$ at very small ground-slopes). On the other hand, for small but fixed γ, the scaling eventually reverts to $p = 1/3$ as ρ approaches zero. The transition occurs when the two left hand side terms above are comparable, or $\rho = \mathcal{O}(\gamma^{2p})$, in which case clearly $p = 1/3$. Thus, the transition occurs when $\rho = \mathcal{O}(\gamma^{2/3})$, or $\gamma = \mathcal{O}(\rho^{3/2})$ as numerically demonstrated in section 4.1.

6.4   Extension of scaling argument to kneed walkers

Kneed walkers dissipate kinetic energy in collisions at both heelstrike and kneestrike. For heelstrike, the energy loss calculations described above still hold: the pre-collision velocities are determined from the straight-legged or two-link configuration, but the matrix $\mathbf{M}$ of equation 9 has to be calculated for the walker in three-link mode since the new swing leg is not constrained at the knee (this has a fairly small effect on $\mathbf{M}$, if the hip mass is relatively large).

For kneed walkers, if the step length is proportional to γ^p, then the collision losses at kneestrike as well as heelstrike are each proportional to either γ^{2p}, or γ^{4p}, or perhaps even higher order, as $\gamma \to 0$. Of these, the heelstrike losses are already known to be at least $\mathcal{O}(\gamma^{4p})$. Thus, the total losses per step are either $\mathcal{O}(\gamma^{2p})$ or $\mathcal{O}(\gamma^{4p})$, leading to $p = 1$ or $p = 1/3$, respectively. In our simulations, zero-slope-capable kneed walkers also have one solution that nearly obeys the high-efficiency ($p = 1/3$) scaling over the range of ground-slopes depicted in the figures. At even smaller ground-slopes, the knee collision eventually dominates and $p = 1$ scaling is recovered, as mentioned in the comments on figure 11 in section 5.2.

Summarizing, in the limit $\gamma \to 0$ both tangential heelstrike and kneestrike have energy dissipation proportional to v^2 and thus dominate the dissipation compared to the hip-deflection related

dissipation (which is proportional to v^4). Thus, both gaits of the kneed walker have a linear scaling between γ and θ^* in the limit $\gamma \to 0$. However, the masses of the legs (as compared to the hip mass) are relatively low, and the link velocity at kneestrike is low, so the speeds at which the kneestrike dissipation dominates the v^4 normal collision are extremely small. Thus, all kneed walkers are mathematically relatively inefficient in the limit $\gamma \to 0$ even though the long step solution has a large range of ground-slopes where it is effectively like an efficient long-step kneeless walker.

7 Chaos in Tuned Kneed Walkers

Like the point-foot walker in Garcia et al. (1996) and Garcia et al. (1998a), and the walkers of Thuilot et al. (1997) and Goswami et al. (1996), we have found here that tuned kneed walkers can also exhibit period doubling and apparently chaotic gait, as shown in figure 12.

At small enough ground-slopes, the period-one gait cycles are stable. The period-one motion becomes unstable at a ground-slope of about 0.084, but a stable period-two gait appears, followed by a stable period-four gait, and so on (see figure 12). The walker continues to have stable persistent walking (that is, not falling down) solutions at ground-slopes of up to about 0.103. At higher ground-slopes we could not find persistent walking motions for this kneed walker. The period-doubling occurs at higher ground-slopes than for the point-foot walker in Garcia et al. (1998a) where the first period-doubling occurs at $\gamma \approx 0.015$ and the chaotic gait is at about $\gamma = 0.019$.

The existence of chaotic motions suggests that the "stepping stone" problem addressed by McGeer (1993) with active torque control might have passive or nearly passive solutions (as also mentioned in Garcia et al. (1998a)). That is to say, many different sequences of short and long steps may be readily available dynamic motions for the walker; and only a small amount of control energy may be needed to move the system trajectory around the chaotic attractor to achieve any desired one of these sequences.

8 Discussion and Conclusions

In agreement with McGeer (1990a) and (1990b), for all the models we studied at every ground-slope, we found no more than two anthropomorphic period-one gait cycles. In our numerical tests, all walkers that pass the statics-based necessary conditions for zero-slope walking (tuning) and have center of mass not too far from the hip, with or without knees, share the following characteristics (see the table in figure 10):

- Two gait solutions exist at all small ground-slopes. That is, the statics based necessary conditions for efficiency optimization seem to be nearly sufficient conditions for perfectly efficient walking.

- For reasons we do not understand (perhaps somehow as an extension of the silly wheel's long-period gait characteristics in McGeer (1993)), the long-step solution is characterized by essentially normal foot collisions. Therefore it has step length $\propto \gamma^{1/3}$ and consumes power P proportional to v^4 at small ground-slopes. This gait is both stable and efficient at small ground-slopes. A small caveat is that, with knees, this solution eventually scales with step length $\propto \gamma$ at extremely small ground-slopes.

- The other solution, characterized by foot collisions with a nonzero tangential component, has step length proportional to γ and consumes power P proportional to v^2 at small ground-slopes. This solution is always unstable. It is more inefficient than the step length $\propto \gamma^{1/3}$

solutions at small ground-slopes. Above some threshold ground-slope, the power scaling for this solution changes to $P \propto v^4$ and step length $\propto \gamma$. This short-step (and shorter period) solution is the faster one at higher ground-slopes when the hip collision dominates collisional losses. (For the simplest walker, the short-step gait is always faster than the long-step gait since there is no tangential foot dissipation).

Although the ground-slopes and specific-costs of transport at which our scalings are numerically observed are below those directly applicable to animals and physical machines, the scalings may shed more light on the fundamental role of collisional loss in the energetics and speed of walking.

Analysis of these simplified models demonstrates the dominance of collisional effects in determining the scaling rules and energy efficiency of their gaits, as for the energetics of collision arguments used for even simpler models by Alexander (the minimal biped) and McGeer (the rimless wheel). Humans and other bipeds may, and do, in fact violate some of our modeling assumptions. Nonetheless, our results give some insight into specific strategies adopted by bipeds, possibly in order to defeat the scaling restrictions suggested by our analysis, particularly the generally dominant power scaling $P \propto v^4$ from hip deflection.

For instance, we noted that the short-step solution is generally faster at high ground-slopes. The tangential collision of this gait could be approximately replaced with a retarding torque at the hip. Thus the higher efficiency of the short-step solution at larger ground-slopes provides an example where negative muscle work is energetically favorable, because it avoids an even greater collisional dissipation. This hip-collision avoidance in fact may be a strategy used by people, who use negative work to increase step frequency and decrease step length when walking at higher speeds.

The big ($P \propto v^4$) hip collision loss can also be avoided by toeing-off immediately before and during heelstrike, as also suggested by McGeer (1993) and Cavagna et al. (1977).

The zero-slope capable mechanisms are non-generic, in that random small parameter adjustments, in particular, fore-aft movement of the thigh and shank centers-of-mass, cause loss of the zero-slope capability. Thus, all of these walkers have dynamics that are hugely dependent on the fore-aft distribution of mass. Human legs do approximately satisfy the necessary zero-slope conditions, in that a completely relaxed leg hangs more or less straight down from the hip. This gives something to look out for in, for example, the design of prosthetic devices.

The existence of various and chaotic gaits for a kneed walker is a curiosity that indicates the possibility of a large repertoire of passive motions.

There seems to be no objective reason to think ahead of time that a given McGeer-like mechanism will have periodic anthropomorphic gaits. So it is perhaps a credit to the overall human design, that (once one has appropriate search procedures) it is easy to find parameters where the equation $\mathbf{f}(\boldsymbol{\theta}^*) = \boldsymbol{\theta}^*$ has solutions, and that these solutions involve interesting motions.

9   Acknowledgements

built physical walking models which help verify, debug, and promote our work. Mario Gomes and Harry Dankowicz each pointed out a knee-unlocking torque in some gaits, and Harry Dankowicz informed our sense of the word "generic." Rudra Pratap did the strobe photography for figure 2, helped correct the stability labeling in the curves on the upper right of figure 8(e), and made editorial suggestions. Frank Moon suggested including some data points from the physical walker in figure 6; both he and Don Bartel read through this paper and made editorial suggestions and critiques, as did Tad McGeer. Lastly, and perhaps most significantly, we had many interesting and motivating discussions with Mike Coleman over the duration of this work.

References

Alexander, R. M. (1995). Simple models of human motion. *Applied Mechanics Review*, 48:461–469.

Basmajian, J. V. and Tuttle, R. (1973). EMG of locomotion in gorilla and man. In *Control of Posture and Locomotion*, pages 599–609. Plenum Press, New York.

Beckett, R. and Chang, K. (1973). An evaluation of the kinematics of gait by minimum energy. *Journal of Biomechanics*, pages 147–159.

Brach, R. M. (1991). *Mechanical Impact Dynamics: Rigid Body Collisions*. John Wiley and Sons, New York.

Brogliato, B. (1996). *Nonsmooth Impact Mechanics: Models, Dynamics and Control*. Springer, London, UK.

Cavagna, G. A., Heglund, N. C., and Taylor, R. (1977). Mechanical work in terrestrial locomotion: Two basic mechanisms for minimizing energy expenditure. *Am. J. Physiol.*, 233(5):R243–R261.

Chatterjee, A. (1997). *Rigid Body Collisions: Some General Considerations, New Collision Laws, and Some Experimental Data*. PhD thesis, Cornell University.

Chatterjee, A. and Garcia, M. (1999). Small slope implies low speed for Mcgeer's passive walking machines. accepted, subject to revision, for *Dynamics and Stability of Systems*.

Chatterjee, A. and Ruina, A. (1998). A new algebraic rigid-body collision law based on impulse space considerations. *Journal Of Applied Mechanics*, 65:939–951.

Coleman, M., Chatterjee, A., and Ruina, A. (1997). Motions of a rimless spoked wheel: A simple 3D system with impacts. *Dynamics and Stability of Systems*, 12(3):139–160.

Coleman, M. J. (1998). *A Stability Study of a Three-dimensional Passive-Dynamic Model of Human Gait*. PhD thesis, Cornell University, Ithaca, NY.

Collins, J. J. (1995). The redundant nature of locomotor optimization laws. *Journal of Biomechanics*, 28:251–267.

Fallis, G. T. (1888). Walking toy ("improvement in walking toys"). U. S. Patent, No. 376,588.

Fowble, J. V. and Kuo, A. D. (1996). Stability and control of passive locomotion in 3D. *Proceedings of the Conference on Biomechanics and Neural Control of Movement*, pages 28–29. Mt. Sterling, Ohio.

Garcia, M. (1999). *Stability, Scaling, and Chaos In Passive-Dynamic Gait Models*. PhD thesis, Cornell University, Ithaca, NY.

Garcia, M., Chatterjee, A., and Ruina, A. (1997). Speed, efficiency, and stability of small-slope 2-d passive dynamic bipedal walking. *Proceedings of the 1998 International Conference on Robotics and Automation*, expanded version in preparation for *Dynamics and Stability of Systems*.

Garcia, M., Chatterjee, A., Ruina, A., and Coleman, M. (1998a). The simplest walking model: Stability, complexity, and scaling. *ASME Journal of Biomechanical Engineering*, 120(2):281–288.

Garcia, M., Ruina, A., Coleman, M., and Chatterjee, A. (1996). Passive-dynamic models of human gait. *Proceedings of the Conference on Biomechanics and Neural Control of Movement*, pages 32–33. Mt. Sterling, Ohio.

Garcia, M., Ruina, A., Coleman, M., and Chatterjee, A. (1998b). Some results in passive-dynamic walking. *Proceedings of the European Mechanics Colloquium on Biology and Technology of Walking*.

Goswami, A., Espiau, B., and Keramane, A. (1997). Limit cycles in a passive compass gait biped and passivity-mimicking control laws. *Journal of Autonomous Robots*, 4:273–286.

Goswami, A., Thuilot, B., and Espiau, B. (1996). Compass-like bipedal robot part I: Stability and bifurcation of passive gaits. *INRIA Research Report No. 2996*.

Howell, G. W. and Baillieul, J. (1998). Simple controllable walking mechanisms which exhibit bifurcations. In *Proceedings of the 37th IEEE Conference on Decision and Control*.

Hurmuzlu, Y. and Moskowitz, G. (1986). The role of impact in the stability of bipedal locomotion. *Dynamics and Stability of Systems*, 1:217–234.

Kuo, A. D. and Bauby, C. E. (1999). Stabilization of balance in 3-d bipedal locomotion. *Workshop On Biology, Mechanics, And Theory Of Walking at ICRA, Detroit, Michigan*.

Lattanzio, H., Kuenzler, G., and Reading, M. (May 1992). Passive dynamic walking. Project Report, Human Power Lab. Cornell University.

McGeer, T. (1990a). Passive dynamic walking. *International Journal of Robotics Research*, 9:62–82.

McGeer, T. (1990b). Passive walking with knees. *Proceedings of the IEEE Conference on Robotics and Automation*, 2:1640–1645.

McGeer, T. (1992). Principles of walking and running. In *Advances in Comparative and Environmental Physiology*. Springer-Verlag, Berlin.

McGeer, T. (1993). Dynamics and control of bipedal locomotion. *Journal of Theoretical Biology*, 163:277–314.

Mochon, S. and McMahon, T. (1980). Ballistic walking: An improved model. *Mathematical Biosciences*, 52:241–260.

Thuilot, B., Goswami, A., and Espiau, B. (1997). Bifurcation and chaos in a simple passive bipedal gait. *IEEE International Conference on Robotics and Automation*.

Winter, D. A. (1987). *The Biomechanics and Motor Control of Human Gait*. University of Waterloo Press.

Yamaguchi, G. T. and Zajac, F. E. (1990). Restoring unasisted natural gait to paraplegics via functional neuromuscular stimulation: A computer simulation study. *IEEE Transactions on Biomedical Engineering*, 37:886–902.
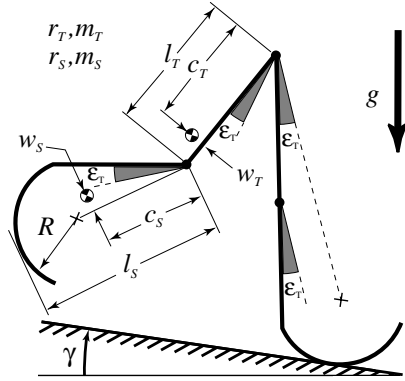
A   Reality Violations in the Simulations

Our numerical simulations are based on various inequality assumptions (see section 2.1), and not a general purpose rigid-body simulation code that checks against interpenetration and tension in contact. Thus, some of the periodic solutions we find might violate various physically-relevant inequality conditions as also discussed in McGeer (1990b). We allow some of those violations in order to have solutions to study over the parameter range of interest. When building a physical model, however, these issues are of interest; we list them below, and in some cases, we include a rationalization for neglecting the item in question.

1. **Foot scuffing.** In simulations of straight-legged walkers, the swing leg inevitably passes through or scuffs the ground near mid-swing. In physical realizations of straight-legged walkers, McGeer overcame this scuffing either with electromechanically-retractable ankles or with tiles placed on the ground (spaced for alternate stance-leg landings). A student group at Cornell University (Lattanzio et al. (1992)) overcame this difficulty using a passive mechanism that slightly retracted the swing leg. Kneed walkers may, but do not necessarily, avoid this scuffing by sufficiently flexing the swing shank at mid step. For 3D walking mechanisms (e. g., Fallis (1888)) and possibly in part for humans, foot scuffing can be avoided by side-to-side rocking. An unpowered scuffing solution could be changed to a non-scuffing solution by adding a small amount of actuation or a passive mechanism to slightly retract alternating legs for clearance.

2. **Positive knee-locking of the stance leg.** In our physical model (figure 2), a joint-stop prevents knee hyperextension, but for practical purposes, nothing stops knee flex. In our simulations we assume that the stance knee is locked until it leaves the ground. Naturally-arising torques at the knee prevent unlocking in some but not all solutions. The simulation shown in figure 3 has a slight stance-leg unlocking impulse at kneestrike which we ignore in our simulations. The corresponding physical model does not collapse, presumably because the naturally-arising torques just after kneestrike are enough to re-engage the knee stop. But even if they might not be, intermittent locking of a rotating joint can be performed with (theoretically) zero energy cost.

3. **Positive stance contact force and no slip.** The simulations assume contact between the stance leg and the ground. There is no contact tension in our simulations since all motions are well below the speed range ($v \approx \sqrt{gL}$) where tension is required to keep the stance leg in contact with the ground. We assume that there is enough friction available to achieve the non-sliding heelstrike collisions assumed by the model. For the physical walkers that we have built, using rubber feet on a linoleum surface, this assumption has turned out to be a reasonable one.

4. **Unlocking of the new swing leg.** As a leg switches from stance to swing in the simulations, we do not allow the leg to hyperextend at the knee. Some non-tuned kneed walkers would exhibit this behavior at very small step lengths if allowed to, but we exclude such solutions.

5. **Ground release of the new swing leg.** As a leg switches from stance to swing (at heelstrike), it is released from the ground. Sometimes at release, the first motion of the swing foot penetrates the ground. Such penetration could be avoided with a low energy ankle retractor.

6. **No stance-foot impulse at heelstrike.** Following McGeer, we assume in our simulations that during the heelstrike collision, no impulse acts on the old stance foot from the

ground. We have not tested this modeling assumption with force plate measurements, but it is self-consistent and gives simulation results which correctly predict the behavior of our experimental models.

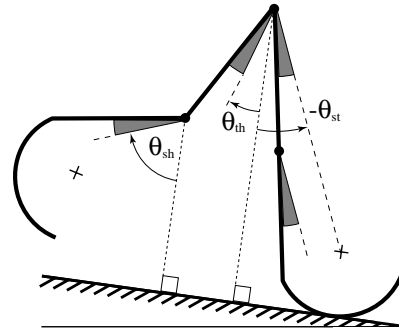a) DIMENSIONAL PARAMETERS   b) DYNAMIC VARIABLES

Figure 1: Our description of McGeer's kneed walking model. Shown above are (a) model parameters, and (b) dynamic variables. Radii of gyration and masses of thigh and shank are denoted by r_t, m_t, r_s, and m_s, respectively. The foot is a circular arc centered at the "+". ε_T is defined to be the angle between the stance thigh and the line connecting the hip to the foot center. Dynamic variable values θ_{st}, θ_{th}, and θ_{sh} are measured from ground-normal to lines offset by ε_T from their respective segments. A stop (not shown) at each knee prevents hyperextension of either knee. In straight-legged models, the knee is locked.
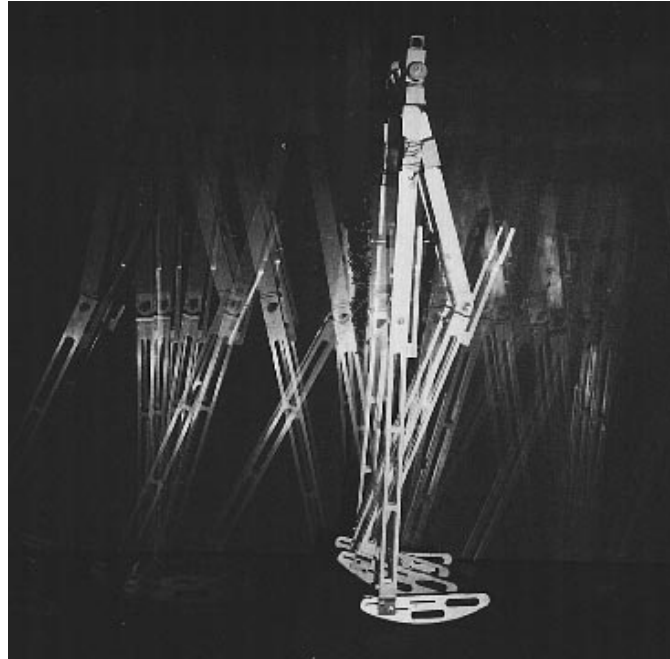
Figure 2: Strobe photo of our McGeer-like mechanism walking down a shallow ramp (not visible under feet). The double leg-set constrains motions to a plane. Plastic collisions at kneestrike and heelstrike are enforced by leaky suction cups at the knees and rubber on the feet, respectively. The simulation of figure 3 uses the parameters of this walker. Photo by Rudra Pratap.
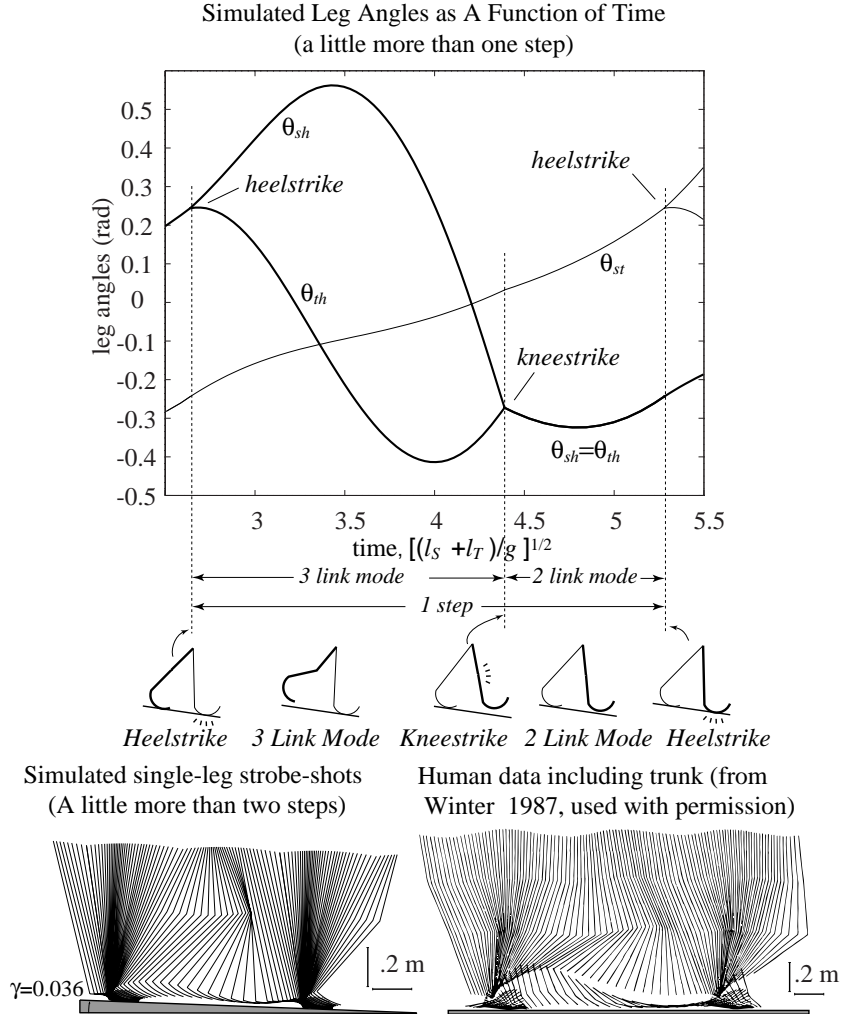
Figure 3: A simulated gait cycle shows leg segment angles from just before a heelstrike to just after the next heelstrike in a steady stable gait (following McGeer). The heavy line on the graph corresponds to the motion of the heavy-line leg on the cartoon under the graph. At the start of the step, it is the stance leg, then becomes the swing leg at the first heelstrike, and again becomes the stance leg after the second heelstrike. Kinks in the curves due to discontinuities in angular velocities at kneestrike and heelstrike are marginally visible. The strobe-like picture of this simulation can be compared to measured human data (with a smaller scale and a longer stride) from Winter (1987). The dimensionless parameters used (from the device in figure 2) are: $l_t = 0.35$m, $w_t = 0$m, $m_t = 2.345$kg, $r_t = 0.099$m, $c_t = 0.091$m, $l_s = 0.46$m, $w_s = 0.025$m, $m_s = 1.013$kg, $r_s = 0.197$m, $c_s = 0.17$m, $R = 0.2$m, $\gamma = 0.036$rad, $g = 9.81$m/s^2, $\varepsilon_T = 0.097$rad.
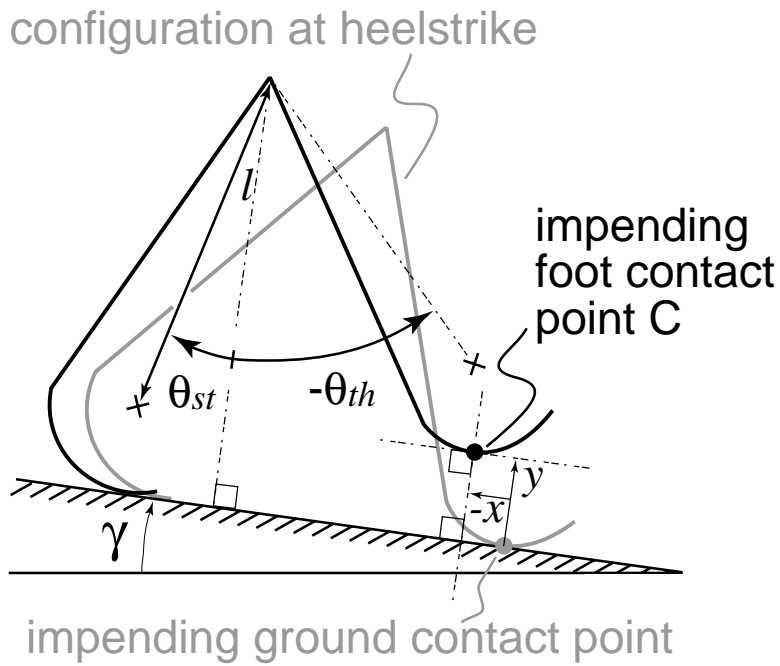
Figure 4: Close to heelstrike, the x and y coordinates of the impending foot contact point C, measured from the impending ground contact point, can be used as generalized coordinates to describe the configuration of the walker. The sizes of x and y are slightly exaggerated for illustration; in the text, they are taken to be small. l is the distance between the foot center and the hip.
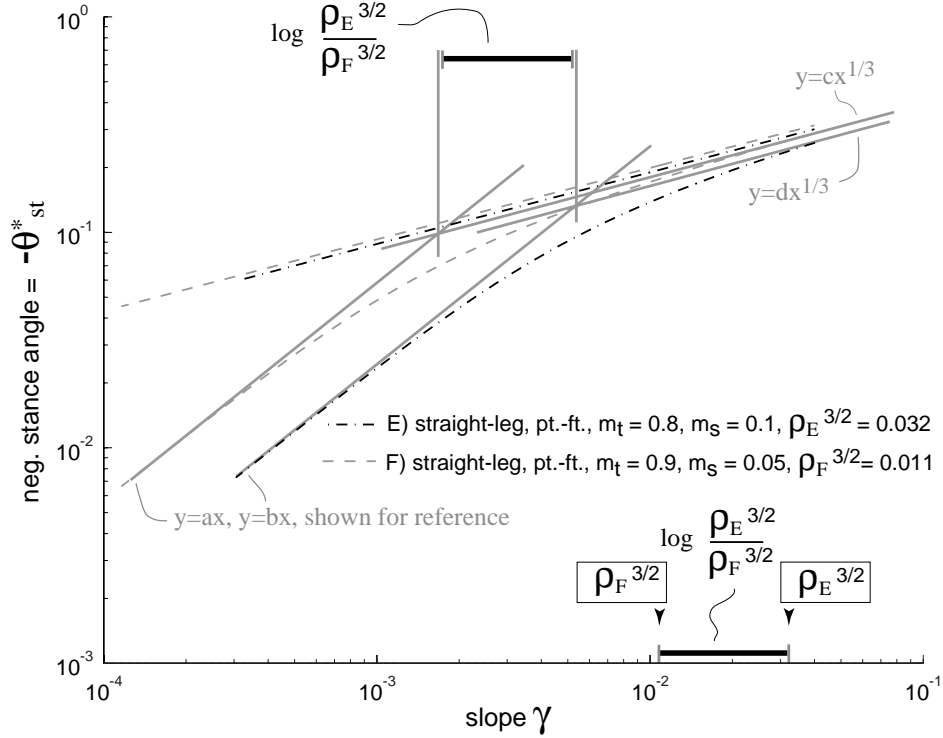
Figure 5: The scaling transition for two point-foot walkers. The foot to total mass ratio for the two walkers are $\rho_E = 0.1$ and $\rho_F = 0.05$. At large ground-slopes ($\gamma \gg \rho^{3/2}$), both gaits of the walkers have step lengths that scale as $\gamma^{1/3}$. At small ground-slopes the short-step step lengths scale as γ. Using the intersection of best-fit straight lines as an estimate of the transition γ values it is seen, consistent with theory, that the ratio of the transition γ values is very close to the ratio of the $\rho^{3/2}$ values. On this plot, the solution curves for the simplest walker would show as parallel lines more or less on top of the upper simulations in this figure.
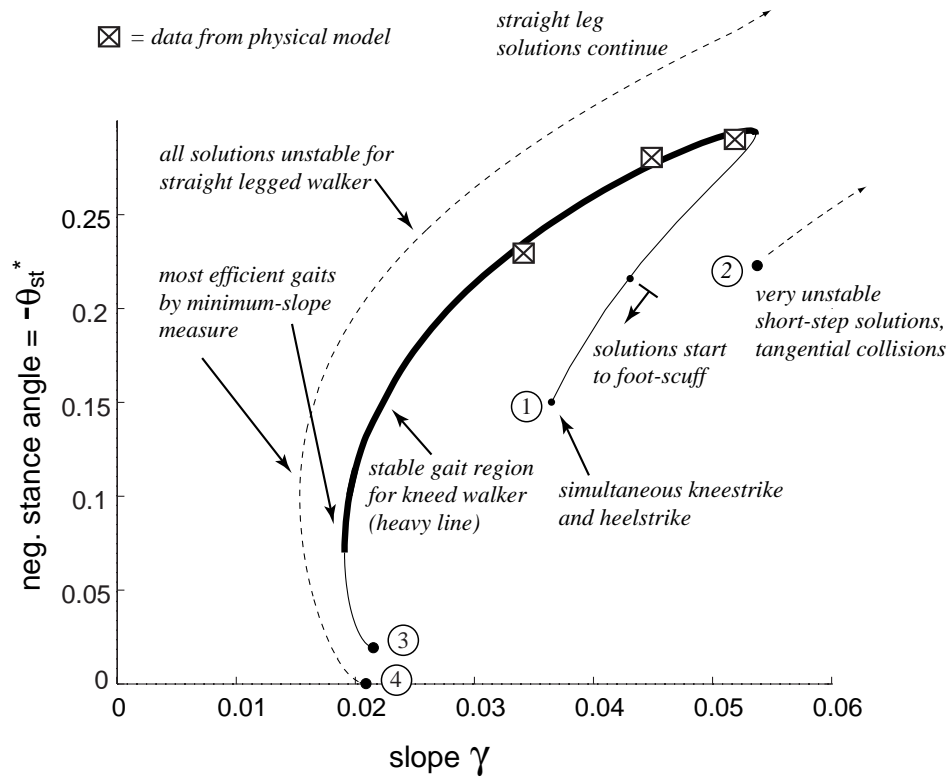
Figure 6: Numerically-calculated locus of solutions showing fixed points of stance angle as a function of ground-slope for our physical kneed walking model (solid line) and for the same model but with the knees locked (dashed line). The thick portion of the solid line denotes stable solutions for the kneed walker. Three data points taken from video recordings of the corresponding physical model are shown with a boxed x.

Conditions for Gait Solutions at Arbitrarily Small Slopes

a) Straight-Legged Walker
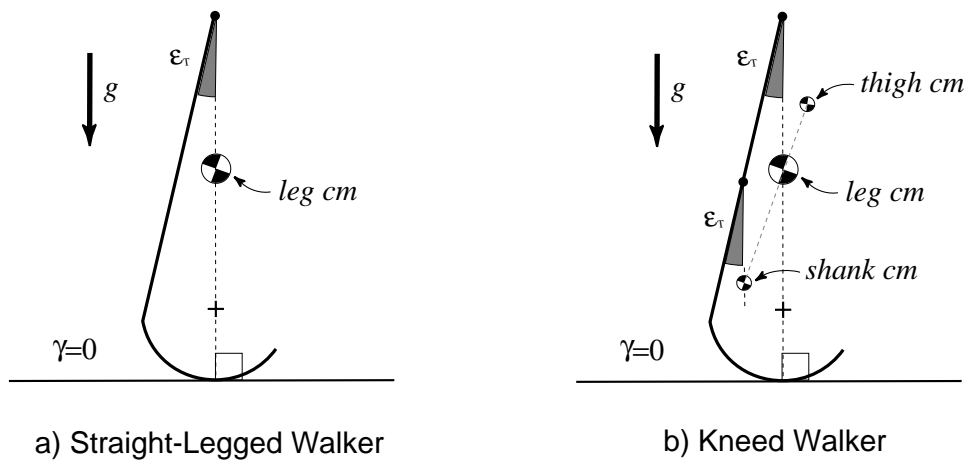
b) Kneed Walker

Figure 7: To walk at arbitrarily shallow ground-slopes, a walker must allow a static standing solution at zero ground-slope with the stance leg locked, the swing leg knee marginally unlocked, the legs parallel, and the hip directly above the foot contact. These conditions are shown graphically for (a) a straight-legged, and (b) kneed walker.
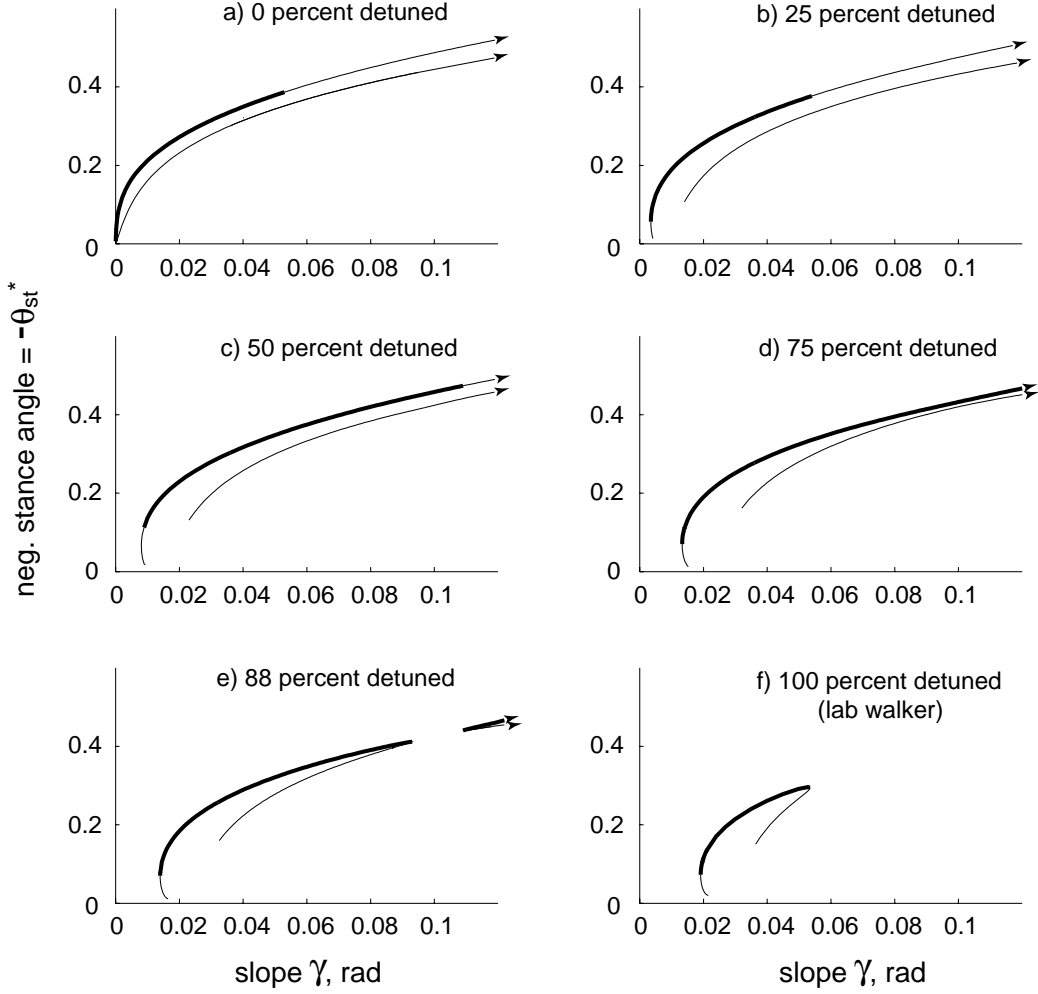
Figure 8: Locus of solutions for various degrees of detuning from (a), a zero-slope (tuned) walker, to (f) the physical walker tested in our lab. The sequence of solutions for the various detunings are described in the text.

Walker	l_t	w_t	m_t	r_t	c_t	l_s	w_s	m_s	r_s	c_s	R	ε_T
A	0.35	-0.023	2.345	0.1882	0.084	0.46	0.022	1.013	0.1226	0.17	0.2	0.097
B	0.5	0	0.4	0	0	0.5	0	0.1	0	0.5	0.2	0
C	0.35	-0.023	2.345	0.1882	0.084	0.46	0.022	1.013	0.1226	0.17	0.2	0.097
D	0.5	0	∞	0	0	0.5	0	1	0	0.5	0	0
E	0.5	0	0.4	0	0	0.5	0	0.1	0	0.5	0	0

Figure 9: Parameters for several tuned walkers in any consistent units. Only C has knees. Straight-legged walkers A, B, D, and E have redundant parameters since the shank and thigh are rigidly connected. m_t and m_s are the thigh and shank masses. For B, D, and E m_s is a point-mass at the bottom of the foot.
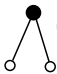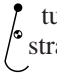
	Zero-Slope Capable?	Short-step scaling ?	Long-step scaling ?	Which soln. faster for $\gamma \rightarrow 0$?	Which soln. faster for larger γ ?	Chaos?
Simplest Walker	Yes	$P \sim v^4$ $\theta^* \sim \gamma^{1/3}$	$P \sim v^4$ $\theta^* \sim \gamma^{1/3}$	Short-Step	Short-Step	Yes
with finite foot mass	Yes	$\left.\begin{array}{l}P \sim v^4\\ \theta^* \sim \gamma^{1/3}\end{array}\right\}$ larger γ $\left.\begin{array}{l}P \sim v^2\\ \theta^* \sim \gamma\end{array}\right\}$ $\gamma \rightarrow 0$	$P \sim v^4$ $\theta^* \sim \gamma^{1/3}$	Long-Step	Short-Step	Not checked
tuned straight-leg	Yes	$\left.\begin{array}{l}P \sim v^4\\ \theta^* \sim \gamma^{1/3}\end{array}\right\}$ larger γ $\left.\begin{array}{l}P \sim v^2\\ \theta^* \sim \gamma\end{array}\right\}$ $\gamma \rightarrow 0$	$P \sim v^4$ $\theta^* \sim \gamma^{1/3}$	Long-Step	Short-Step	Not checked
tuned kneed	Yes	$\left.\begin{array}{l}P \sim v^4\\ \theta^* \sim \gamma^{1/3}\end{array}\right\}$ larger γ $\left.\begin{array}{l}P \sim v^2\\ \theta^* \sim \gamma\end{array}\right\}$ $\gamma \rightarrow 0$	$\left.\begin{array}{l}P \sim v^4\\ \theta^* \sim \gamma^{1/3}\end{array}\right\}$ larger γ $\left.\begin{array}{l}P \sim v^4\\ \theta^* \sim \gamma^{1/3}\end{array}\right\}$ small γ $\left.\begin{array}{l}P \sim v^2\\ \theta^* \sim \gamma\end{array}\right\}$ $\gamma \rightarrow 0$	Long-Step	Short-Step	Yes

Figure 10: Summary of the properties of various walkers capable of walking at arbitrarily small ground-slopes. In this table, as in the text, P refers to the power required for walking at a gait limit cycle, v is the average velocity of the walker, θ^* is the stance angle at the start of a gait cycle, and γ is the ground-slope. The term "larger γ" refers to ground-slopes that are above the transition ground-slope, as discussed in subsection 6.3; these transition ground-slopes are different for each particular walker and gait solution. The tuned kneed walker has three slope categories listed because the scaling transition only occurs at *extremely* small slopes, as explained in the text.
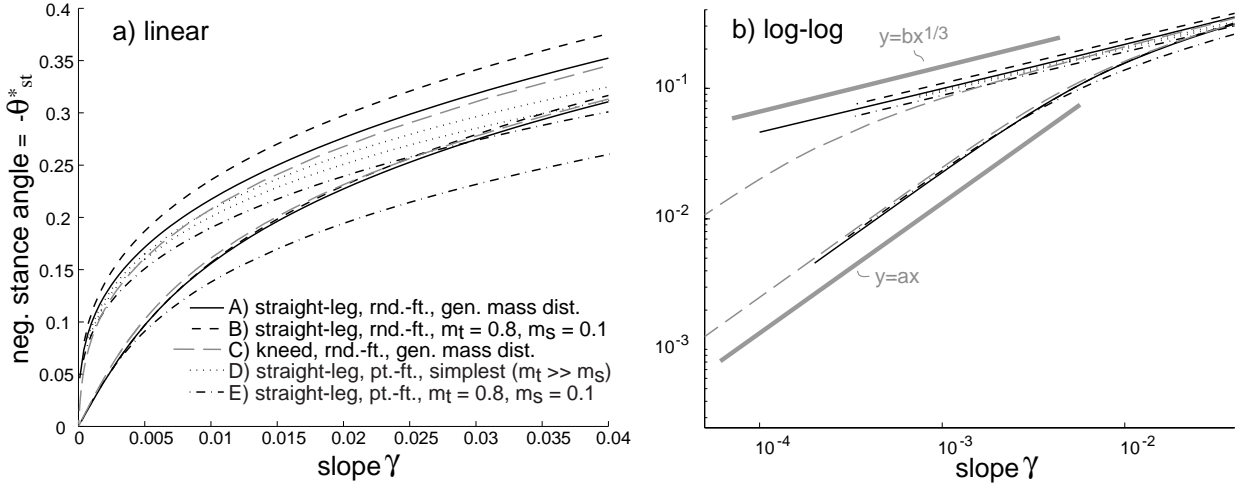
Figure 11: Gait families for tuned zero-slope-capable walkers on (a) a linear plot, and (b) a log-log plot. Parameter values are listed in table 1. By "gen. mass. dist." is meant that the parameters were similar to those of the kneed walker of figure 3. Note (1) there are two gaits cycles at each γ for all walkers shown; (2) for the "simplest" walker (D) both step lengths are proportional to $\gamma^{1/3}$; (3) the short-step gaits of the other walkers have step lengths proportional to γ for small γ; (4) the long-step gaits for the other walkers have step lengths that are much longer than for the short-step gaits, though not necessarily exactly proportional to $\gamma^{1/3}$ for small γ; and (5) for a point-foot, straight-legged walker with non-negligible foot mass, the step length of the long-step gait *is* proportional to $\gamma^{1/3}$ for small γ. The scaling results are the same when plotted against average forward velocity instead of stance angle, but some of the relative heights of the short-step and long-step solutions are not preserved (some short-step solutions are faster than long-step solutions at large γ, and for all γ for the simplest walker).
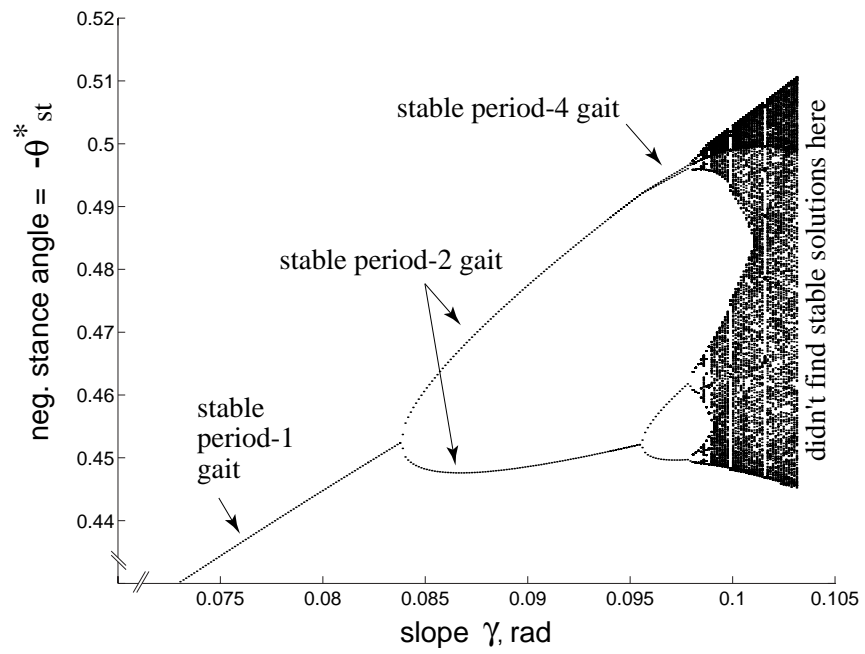
Figure 12: Period doubling of stable kneed walking motions. Only stable walking motions are shown, although unstable gait cycles continue for larger values of γ. The parameters are those of the tuned kneed walker (C) in table 1.